A novel fibre-optic pore pressure sensor for soil element testing

Chao, C.; Parra-Gómez, L. J.; Muraro, S.; Broere, W.; Jommi, C.

DOI
10.1680/jgele.24.00088

Publication date
2025

Document Version
Final published version

Published in
Geotechnique Letters

Chao, C. *et al.* (2025) ***Géotechnique Letters*** **15**, 000–000, https://doi.org/10.1680/jgele.24.00088

A novel fibre-optic pore pressure sensor for soil element testing

C. CHAO*, L. J. PARRA-GÓMEZ*, S. MURARO*, W. BROERE* and C. JOMMI*†

Interpretation of element testing in soil mechanics can be enhanced to a large extent with the use of local pressure measurements, helping in quantifying the consequences of non-uniform stress, strain, and pore pressure fields within the sample. Available diaphragm pressure transducers can be useful to this aim; however, they suffer from several limitations. A novel Fabry–Pérot fibre-optic sensor for local measurement of pore water pressure within the sample is presented and discussed. The sensor addresses several limitations of current mid-plane diaphragm transducers, including long-term drifting, temperature sensitivity, and maintenance difficulties. The new sensor offers significant advantages in terms of reduced sample disturbance, data acquisition frequency, and response time.

KEYWORDS: fibre-optic transducer; laboratory tests; local sensors; pore pressures

INTRODUCTION

Accurate pore water pressure measurement within soils is crucial for assessing their hydro-mechanical coupled response. In traditional triaxial apparatuses, pore water pressure is measured using a transducer connected to the bottom or top of the sample. However, several studies have highlighted that this arrangement introduces uncertainties in pore pressure measurement due to end restraint effects, influencing effective stress determination and thereby affecting test results interpretation (Blight, 1964; Bishop & Green, 1965; Fourie & Xiaobi, 1991; Feda *et al.*, 1993; Schanz & Gussmann, 1994; Sheng *et al.*, 1997; Jeremić *et al.*, 2004; Kodaka *et al.*, 2007; Muraro & Jommi, 2019).

To alleviate end restraint effects, tests are typically conducted with smooth platens or at sufficiently slow rates. However, recent studies have shown that for soft soils, this equalisation can be difficult as their large deformations exacerbate the effects of end restraint and result in a non-homogeneous deformation field within the sample (Muraro & Jommi, 2021). The adoption of smooth platens also has practical limitations. Their use requires modifications to the experimental setup that complicate the sample mounting procedure and generate potential geometrical instabilities (Mozaffari *et al.*, 2022). In addition, they cannot be fully implemented when bender elements or high air-entry value porous disks are required.

Alternatively, local pore pressure transducers can measure and allow accounting for non-uniform pore pressure inside the sample. Local piezometer probes were first introduced by Taylor (1940) for triaxial tests. However, as noted by Hight (1982), the first versions of the sensor encountered installation difficulties and a high failure rate. Hight (1982) subsequently developed a miniature silicon diaphragm pressure transducer, which effectively monitored pore pressure under both monotonic and cyclic loading conditions. However, the new design suffered from potential interference between the protective porous stone and the sensing unit. Modern commercially available sensors use diaphragm transducers behind a porous stone disk, which require long saturation procedures to minimise biases in pore pressure measurements. In addition, they are meant to be mounted on the lateral surface of the sample, which makes them susceptible to the boundary effects that arise from the folding or stretching of the latex membrane during testing.

One possible way to address these limitations lies in the use of miniature fibre-optic pressure sensors that have become increasingly common in other areas, particularly in the medical field. In geotechnical engineering, these sensors have been used to monitor pore pressure generation at the pile–soil interface in centrifuge tests (Askarinejad *et al.*, 2020; Nietiedt *et al.*, 2024). However, to the best of the authors' knowledge, their feasibility for soil element testing has not been explored yet. The fabrication and application of a miniature fibre-optic pore pressure sensor in triaxial testing are presented. The developed sensor reliably measures pore water pressure over the height of the specimen, with minimal long-term drift, reduced sensitivity to environmental variations, and fast response suitable for cyclic testing. Its small size and lightweight minimise sample disturbance during installation, and modularity eases its maintenance.

FIBRE-OPTIC PORE PRESSURE SENSOR

The local fibre-optic pore pressure sensor discussed here was constructed using the FOP-M R2 fibre-optic transducer from FISO, which utilises white-light Fabry–Pérot interferometry technology and measures pressure based on the micro-opto mechanical system (Pinet, 2009). When pressure is applied, the diaphragm deflects, reducing the cavity length as schematised in Fig. 1. It is important to note that the glass cavity is vacuum-sealed, meaning that the sensor provides total pressure readings.

The dimensions of the FOP-M R2 fibre-optic pressure transducer are also depicted in Fig. 1. The 10 mm long sensing tip requires protection from bending moments or mechanical loads. The detailed drawings of the sensor assembly with protection casing are presented in Fig. 2. The

Manuscript received 26 June 2024; accepted 30 May 2025.
*Department of Geoscience and Engineering, Delft University of Technology, Delft, The Netherlands.
†Department of Civil and Environmental Engineering, Politecnico di Milano, Milano, Italy.

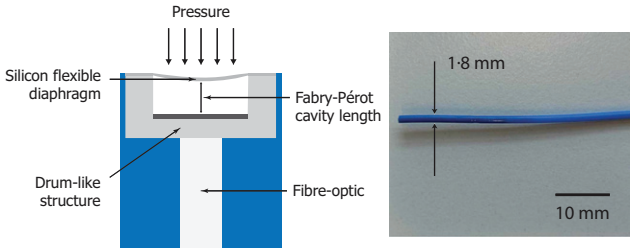

Fig. 1. Working principle and dimensions of the fibre-optic pressure sensor (after Pinet, 2009)

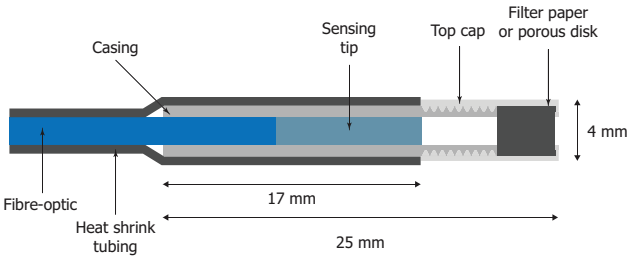

Fig. 2. Detailed schematic of the FOP sensor assembly with protection casing

threaded front end of the casing accommodates various tip caps, providing flexibility for different test types (e.g. saturated and unsaturated) and facilitating sensor tip maintenance. A porous stone or filter paper can be used as protection for the tip of the sensor. A FISO EVOLUTION signal conditioner with a maximum sampling rate of 125 Hz is used for fast data acquisition, offering an accuracy of 1·72 kPa and a resolution of 0·172 kPa with the adopted sensor.

The fibre-optic pore pressure sensor assembly has a 4 mm dia., minimising installation disturbance and significantly reducing the leakage risk through the membrane. The casing enables the sensing tip to be placed inside the sample, and the decreased weight and miniaturised design facilitate the installation of multiple devices on a single specimen.

SENSOR RELIABILITY AND CALIBRATION

The performance of the fibre-optic sensor (FOP) under varying environmental conditions was benchmarked against a commercially available mid-plane diaphragm transducer (MP). Both sensors were placed underwater at atmospheric pressure inside a chamber with controlled temperature and relative humidity (RH); the dimensions of the chamber and the layout of the benchmark setup are shown in Fig. 3. Outside the chamber, the room temperature is regulated to 15°C. The manometric changes in the FOP and MP sensors were computed by subtracting the atmospheric pressure recorded by an independent transducer. During the first 3 days, the fibre-optic interrogator was kept outside the chamber to measure the effects of temperature differentials with the sensor tip (Fig. 3(a)). The interrogator was then moved inside the chamber to assess the influence of temperature and RH (Fig. 3(b)).

Figure 4 shows the time series measurements of the manometric pressure in both transducers, temperature and RH. It can be seen that temperature changes of 10°C caused changes of about 2·0 kPa in the MP sensor. In contrast, while the sensing unit was separated from the sensing tip, the FOP recorded a maximum pressure drop of 0·2 kPa. After the sensing box was placed in the chamber, subsequent

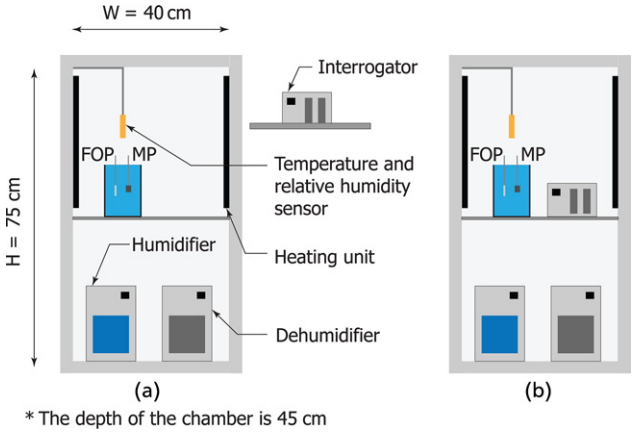

Fig. 3. The dimensions of the chamber and the layout of the benchmark setup: (a) interrogator outside the chamber; (b) interrogator inside the chamber

temperature changes caused small transient spikes in the pressure recordings, which quickly equalised. The FOP changes appear to be positively correlated with the change in temperature, while the MP is affected oppositely. An interesting observation is that under the isothermal and isohumic conditions maintained from day 8 onwards, the MP sensor appeared to drift at a constant rate. Evidence of this drift has been observed during real testing conditions, and it appears to be smaller for the FOP.

Linear regression and analysis of variance were performed to quantify the qualitative observations. The manometric outputs of both transducers were modelled using temperature (T), RH, and elapsed time (t) in days as independent variables. All series were found to be non-stationary and integrated of order one, I(1). Consequently, the influence of elapsed time was assessed using the model for integrated values shown in Equation 1 (FOP 1 and MP 1), while the effects of T and RH were modelled by their first differences as described in Equation 2 (FOP 2 and MP 2). Table 1 summarises the findings.

$$y = \beta_0 + \beta_1 T + \beta_2 RH + \beta_3 t \quad (1)$$

$$\Delta y = \beta_0 + \beta_1 \Delta T + \beta_2 \Delta RH + \beta_3 \Delta t \quad (2)$$

The analysis shows that the RH effects are small for the MP (−13·9 Pa/%) and statistically insignificant for the FOP. The temperature effects are significant for both sensors, but the magnitude is almost 50 times smaller in the FOP compared with the MP, with values of −2·7 and 125 Pa/°C, respectively. Notably, the MP 1 model shows that accounting for temperature and RH changes, the MP shows a drift of 432 Pa/day. Such a value amounts to a significant measurement error over long testing times. In comparison, the FOP drifts by −7·20 Pa/day, showing the improved stability of the recordings.

The sensor output was tested in a triaxial apparatus using a calibration loading–unloading ramp up to a manometric pressure of 650 kPa. The fibre-optic pressure sensor was zeroed before the pressure increase to ensure that all sensors in the apparatus had the same pressure reference. Due to the short duration of the procedure, the measurements were not significantly affected by changes in atmospheric pressure. However, for long-term tests, it is recommended to adjust the FOP measurements with an independent total atmospheric pressure sensor. The results of the calibration ramp, plotted in Fig. 5, show that the sensor performance exhibits adequate linearity within the tested pressure range. Measurement differences relative to the controlled cell pressure

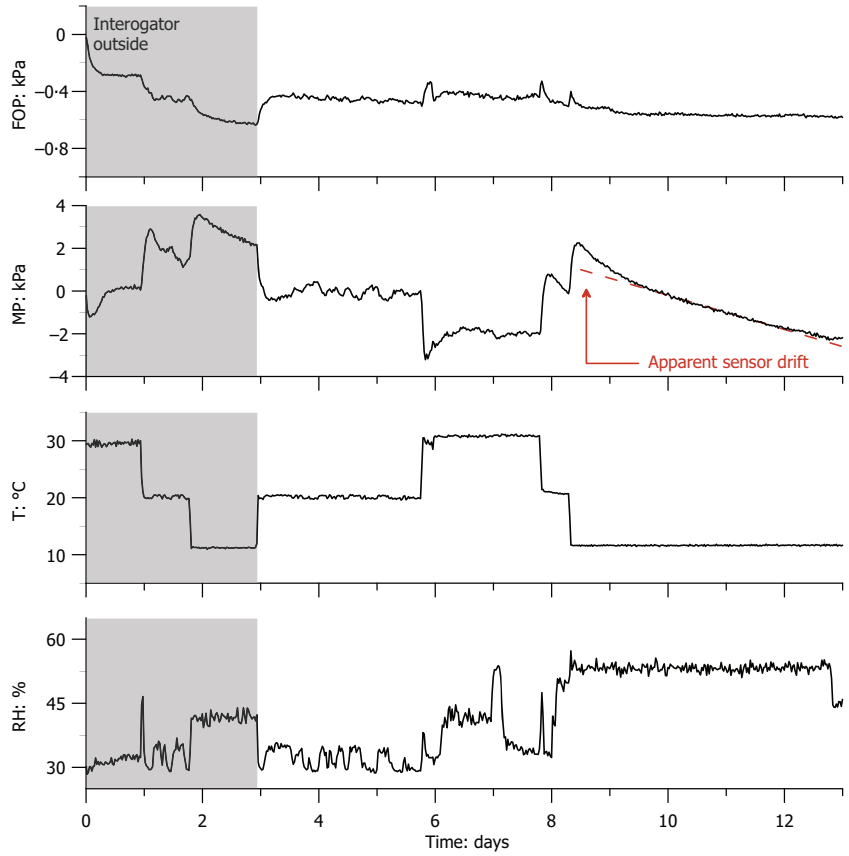

Fig. 4. Time evolution of the manometric pressures recorded by the FOP and MP transducers, temperature, and relative humidity

Table 1. Summary of sensor reliability assessment

Model	R^2	β_0: kPa	β_1 (T): kPa/°C	β_2 (RH): kPa/%	β_3 (t): kPa/day
FOP 1	0·724	$-6{\cdot}09 \times 10^{-1}$	$8{\cdot}60 \times 10^{-3}$	$3{\cdot}00 \times 10^{-4}$*	$-7{\cdot}20 \times 10^{-3}$
FOP 2	0·024	$3{\cdot}10 \times 10^{-3}$*	$-2{\cdot}70 \times 10^{-3}$	$-4{\cdot}00 \times 10^{-4}$*	$-1{\cdot}95 \times 10^{-1}$*
MP 1	0·810	3·81	$-1{\cdot}50 \times 10^{-1}$	$3{\cdot}87 \times 10^{-2}$	$-4{\cdot}32 \times 10^{-1}$
MP 2	0·340	$-1{\cdot}40 \times 10^{-3}$*	$-1{\cdot}25 \times 10^{-1}$	$-1{\cdot}39 \times 10^{-1}$	$-2{\cdot}32 \times 10^{-1}$*

*Coefficient is not statistically significant (t-test p-value >0·05)

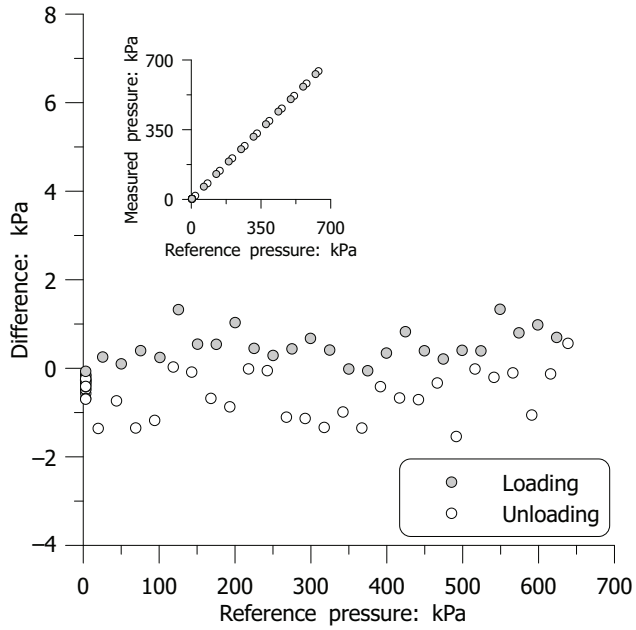

Fig. 5. Results of the calibration ramp for the FOP sensor

were below 1·5 kPa, which is consistent with the accuracies reported in the specifications of both devices.

PROOF OF CONCEPT

The new sensor capabilities were tested in a triaxial setup using an undisturbed sample of Dutch organic clay retrieved from the Leendert de Boerspolder in the Netherlands (Jommi *et al.*, 2021; Ponzoni *et al.*, 2024). Three sensor assemblies were installed at different heights of the soil sample (z/H = 0·2, 0·5, and 0·8) using silicone rubber connectors, as illustrated in Fig. 6. The initial sample size was 50 mm in diameter and 100 mm in height. The sensors were installed at three different positions along the circumference to avoid membrane interference. O-rings were used to seal the sensor shaft inside the connector. Small holes, 3 mm wide and 5 mm deep, were drilled, and the sensing tips were installed 5 mm inside the soil sample to minimise boundary effects from the deformation of the latex membrane.

The sample was isotropically consolidated to a mean effective stress of 50 kPa and then subjected to 25 axial strain cycles with an amplitude of 0·15% at a frequency of 0·001 Hz. After post-cyclic consolidation, the sample was sheared in undrained compression at a relatively fast axial strain rate of 0·1%/min.

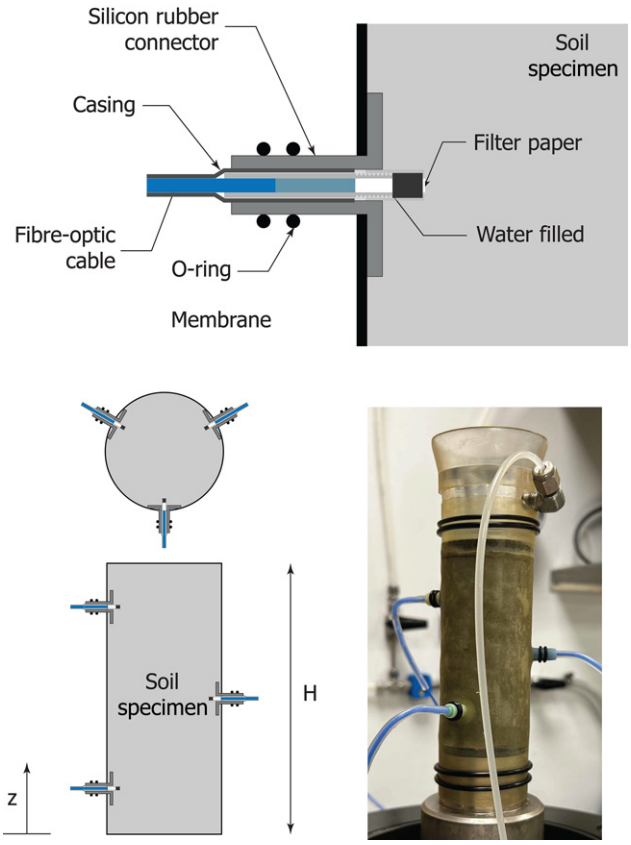

Fig. 6. Installation details of the FOP sensor assembly on the soil specimen

The isotropic consolidation stage was performed by rapidly increasing the cell pressure to the target value, only allowing drainage from the top boundary of the sample. Figure 7 presents the time history of the excess pore pressure measured by three FOP sensors at different heights. The excess pore pressure profile in the sample is also shown in Fig. 7. The results demonstrate that the FOP sensors can effectively track the consolidation process within the sample.

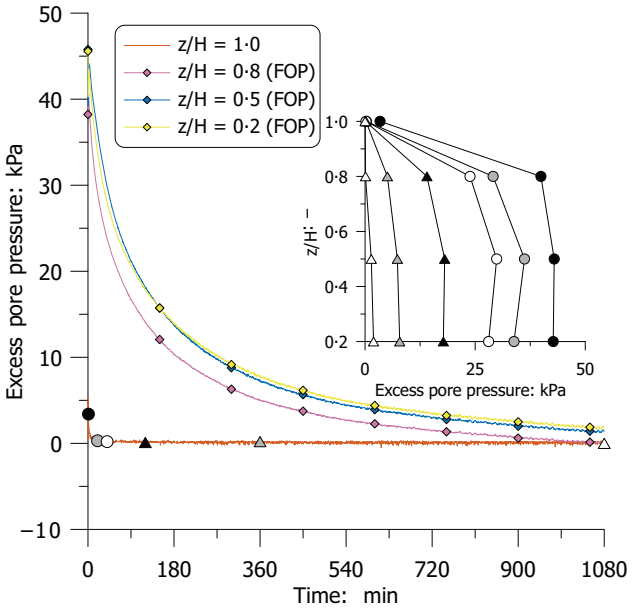

Fig. 7. Excess pore pressures recorded by the FOP sensors during the isotropic consolidation stage

To validate sensor performance upon loading reversal, Fig. 8 presents the axial strain and the excess pore pressure recorded by the transducers at the boundaries ($z/H = 0$ and 1) and the FOP sensors during cyclic loading. The data show no discernible differences in phase or value between the sensors, suggesting that the FOP sensors have a short enough response time to reliably track the result of the coupled hydro-mechanical response of slow cyclic loading.

Figure 9 illustrates the excess pore pressure during the final monotonic shearing stage. The comparison between the different sensors during the pre-failure stage reveals 2–3 kPa higher excess pore pressures at the sample extremities due to end-restraint, with the lowest value observed at mid-height. Following the onset of failure at approximately 7% axial

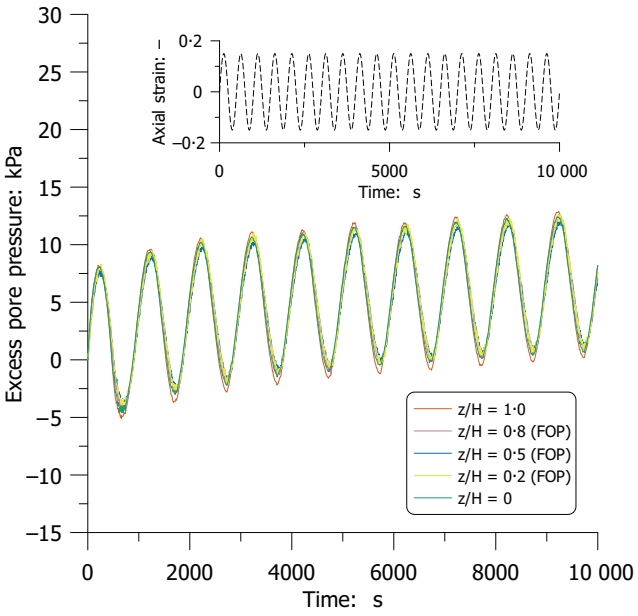

Fig. 8. Excess pore pressures recorded by the FOP sensors and the pore pressure transducers at the extremities during strain-controlled undrained cyclic triaxial stage

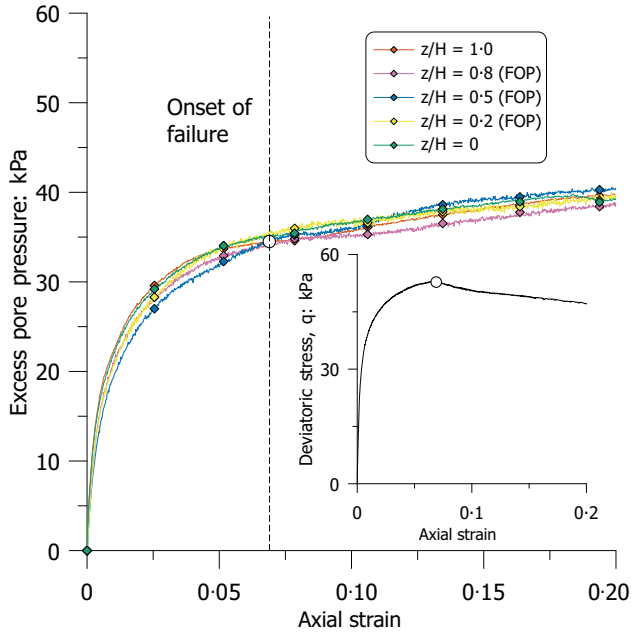

Fig. 9. Excess pore pressures recorded by the FOP sensors and the pore pressure transducers at the extremities during monotonic undrained triaxial compression

strain, the evolution of excess pore pressure becomes more complex due to the non-uniform deformation mode accentuated by the large strains. The experimental observations confirm the reliability of the proposed FOP in measuring pore pressure over the height of the sample and show that the sensors can provide valuable insight for test interpretation.

CONCLUSIONS

This study introduces a novel miniature fibre-optic local pore pressure sensor for soil element testing. The sensor was compared with a commercially available traditional diaphragm transducer, demonstrating clear performance enhancement. Statistical analysis reveals that the proposed device exhibits a significant reduction in overall long-term drift, statistically insignificant effects from RH, and temperature drifts of 2 Pa/°C, approximately 50 times smaller than those of the reference transducer. In addition, the sensor shows adequate linearity in manometric pressure ranges up to 650 kPa, with absolute errors below 1·5 kPa.

The compact size and lightweight design of the casing minimise sample disturbance and allow placement within the soil sample. Its assembly design offers flexibility for implementation in various test types and facilitates maintenance. The proposed device is a total pressure transducer, and thus, it is recommended to reference its measurements to an independent atmospheric pressure recording when using it for long-term testing.

The sensor performs well in both cyclic and monotonic triaxial tests. In cyclic conditions, it rapidly records pressure data without perceptible delays. During undrained triaxial compression, the sensor reliably captures the local pore pressure field within the sample.

The proposed sensor demonstrates the application of fibre-optic sensing technology and represents a significant advancement over traditional mid-plane diaphragm transducers. Given its small size and flexibility, the sensor could be integrated into many different types of testing apparatuses or experimental setups. Further research is needed to evaluate and validate its performance across different soil types and testing conditions, including cyclic tests at higher frequencies.

DATA AVAILABILITY

The data generated during or analysed during the current study are available from the corresponding author upon request.

ACKNOWLEDGEMENTS

The financial support of the Dutch Organisation for Scientific Research (NWO), under the project 'SOFTTOP: Investigating heterogeneous soft top soils for wave propagation, cyclic degradation and liquefaction potential' with project number DEEP.NL.2018·006, and 'Peatland: living on a gassy soil. Revealing the role of gas on the behaviour of peats' with project number Veni AES 2021·19077 is gratefully acknowledged.

REFERENCES

Askarinejad, A., Quinten, T. O., Grima, M. A., Van't Hof, C. & Gavin, K. (2020). Use of optical fibres to measure pore water pressure development during impact pile diving: a geotechnical centrifuge study. In *European Conference of Physical Modelling in Geotechnics*, pp. 243–246.

Bishop, A. W. & Green, G. E. (1965). The influence of end restraint on the compression strength of a cohesionless soil. *Geotechnique* **15**, No. 3, 243–266.

Blight, G. E. (1964). The effect of nonuniform pore pressures on laboratory measurements of the shear strength of soils. In *Laboratory shear testing of soils*, ASTM International.

Feda, J., Bohac, J. & Herle, I. (1993). End restraint in triaxial testing of soils. *Acta Technica CSAV* **38**, 197.

Fourie, A. B. & Xiaobi, D. (1991). Advantages of midheight pore pressure measurements in undrained triaxial testing. *Geotech. Test. J.* **14**, No. 2, 138–145.

Hight, D. W. (1982). A simple piezometer probe for the routine measurement of pore pressure in triaxial tests on saturated soils. *Géotechnique* **32**, No. 4, 396–401.

Jeremić, B., Yang, Z. & Sture, S. (2004). Numerical assessment of the influence of end conditions on constitutive behavior of geomaterials. *J Eng Mech* **130**, No. 6, 741–745.

Jommi, C., Sterpi, D., de Gast, T., Muraro, S., Ponzoni, E. & van Hemert, H. (2021). Coupled hydro-mechanical analysis of the pre-failure and the failure behaviour of a dyke on soft subsoil: formulation and synthesis of results. In *Numerical Analysis of Dams: Proceedings of the 15th ICOLD International Benchmark Workshop 15*, pp. 645–665. Springer International Publishing.

Kodaka, T., Higo, Y., Kimoto, S. & Oka, F. (2007). Effects of sample shape on the strain localization of water-saturated clay. *Num Anal Meth Geomechanics* **31**, No. 3, 483–521.

Mozaffari, M., Liu, W. & Ghafghazi, M. (2022). Influence of specimen nonuniformity and end restraint conditions on drained triaxial compression test results in sand. *Can Geotech J* **59**, No. 8, 1414–1426.

Muraro, S. & Jommi, C. (2019). Implication of end restraint in triaxial tests on the derivation of stress–dilatancy rule for soils having high compressibility. *Can Geotech J* **56**, No. 6, 840–851.

Muraro, S. & Jommi, C. (2021). Experimental determination of the shear strength of peat from standard undrained triaxial tests: correcting for the effects of end restraint. *Géotechnique* **71**, No. 1, 76–87.

Nietiedt, J. A., Randolph, M. F., Gaudin, C. & Doherty, J. P. (2024). Development of a high-energy centrifuge model impact hammer for pile-driving. *Int. J. Phys. Modell. Geotech.* **24**, No. 2, 56–65.

Pinet, É. (2009). Fabry-Pérot fibre-optic sensors for physical parameters measurement in challenging conditions. *J. Sens.* **2009**, No. 1, 720980.

Ponzoni, E., Muraro, S., Nocilla, A. & Jommi, C. (2024). Deformational response of a marine silty-clay with varying organic content in the triaxial compression spaces. *Can Geotech J* **61**, No. 9, 1819–1831.

Schanz, T. & Gussmann, P. (1994). The influence of geometry and end restraint on the strength in triaxial compression in numerical simulations. In *European Conference on Numerical Methods in Geotechnical Engineering*, pp. 129–133.

Sheng, D., Westerberg, B., Mattsson, H. & Axelsson, K. (1997). Effects of end restraint and strain rate in triaxial tests. *Comput. Geotech.* **21**, No. 3, 163–182.

Taylor, D. W. (1940). *Soil Mechanics Research Program on Cylindrical Compression Testing in Cooperation with US Engineering Department*, Massachusetts Institute of Technology 3rd Report.